Reducing Truck Emissions and Improving Truck Fuel Economy via Intelligent Transportation System Technologies

January 2018

A Research Report from the National Center for Sustainable Transportation

Petros Ioannou, University of Southern California

Yihang Zhang, University of Southern California

National Center for Sustainable Transportation

METRANS Transportation Center
USC | CSULB

About the National Center for Sustainable Transportation

The National Center for Sustainable Transportation is a consortium of leading universities committed to advancing an environmentally sustainable transportation system through cutting-edge research, direct policy engagement, and education of our future leaders. Consortium members include: University of California, Davis; University of California, Riverside; University of Southern California; California State University, Long Beach; Georgia Institute of Technology; and University of Vermont. More information can be found at: ncst.ucdavis.edu.

U.S. Department of Transportation (USDOT) Disclaimer

The contents of this report reflect the views of the authors, who are responsible for the facts and the accuracy of the information presented herein. This document is disseminated under the sponsorship of the United States Department of Transportation's University Transportation Centers program, in the interest of information exchange. The U.S. Government assumes no liability for the contents or use thereof.

Acknowledgments

This study was funded by a grant from the National Center for Sustainable Transportation (NCST), supported by USDOT through the University Transportation Centers program. The authors would like to thank the NCST and USDOT for their support of university-based research in transportation, and especially for the funding provided in support of this project.

NCST

Reducing Truck Emissions and Improving Truck Fuel Economy via Intelligent Transportation System Technologies

A National Center for Sustainable Transportation Research Report

January 2018

Petros Ioannou, Department of Electrical Engineering, University of Southern California

Yihang Zhang, Department of Electrical Engineering, University of Southern California

NCST

[page left intentionally blank]

TABLE OF CONTENTS

List of Figures

Reducing Truck Emissions and Improving Truck Fuel Economy via Intelligent Transportation System Technologies

EXECUTIVE SUMMARY

The aim of this project is to use intelligent transportation system (ITS) technologies that take into account the presence of trucks in the traffic flow, in order to improve impact on the environment by reducing fuel consumption and pollution levels in areas where the truck volume is relatively high. The work is divided into two parts.

In the first part, we propose an integrated variable speed limit (VSL), ramp metering (RM) and lane change (LC) controller using feedback linearization. The proposed integrated controller keeps the bottleneck flow at the maximum level and homogenizes the density and speed of the traffic flow along the highway sections. This improvement of the traffic flow characteristics lead to improved fuel economy and reduction in tailpipe emissions of both trucks and passenger vehicles. In order to evaluate the performance of the integrated traffic controller, a microscopic traffic simulation network of the I-710 highway, which is connected to the Ports of Long Beach/Los Angeles and has high truck volume, is developed. We use Monte-Carlo traffic flow simulations to demonstrate that the integrated traffic controller can generate consistent improvements with respect to travel time, safety, fuel economy and emissions under different traffic conditions.

In the second part, we compared the proposed feedback linearization controller with the widely-used model predictive traffic controller in terms of performance and robustness with respect to perturbations on traffic demand, model parameters and measurement noise. Results show that both controllers are able to improve the total time spent, which leads to improvements in fuel economy and emissions, under different levels of perturbation and noise. The feedback linearization controller however, guarantees good performance and robustness properties than the model predictive controller with much less computational effort.

Chapter 1: Integrated Control of Highway

Introduction

Highway congestion is detrimental to traffic mobility, safety and the environment. To prevent or relieve highway congestion, different Intelligent Transportation System (ITS) techniques, e.g. dynamic routing, driver information systems, variable speed limit (VSL), ramp metering (RM) etc., are widely studied and used to improve the efficiency of existing road networks (Lu, Varaiya, Horowitz, Su, & Shladover, 2011; Papageorgiou, Hadj-Salem, & Middelham, 1997; Zhang & Ioannou, 2017a, 2017b, 2017c).

Due to the variety and complexity of underlying causes of highway congestion, such as excessive mainline and ramp demand, shockwaves, capacity drop etc., developing traffic control techniques that cover all possible cases is a challenging task. A variety of control techniques have been proposed for highway traffic flow control. These include variable speed limit (VSL), ramp metering (RM) and lane change (LC) control. Variable speed limit dynamically changes the speed limits along a highway segment in an effort to regulate the traffic flow and improve traffic conditions at the bottlenecks. Ramp metering limits the number of vehicles entering the highway from on-ramps in order to maintain an appropriate demand on the highway and attenuate the disturbance of ramp flows to the mainline. Lane change control provides lane change instructions to vehicle drivers by efficiently distributing vehicles to open lanes. For general traffic flow, fuel consumption and pollution rate can be reduced by reducing total time spent by vehicles on road and homogenizing the traffic flow thereby reducing unnecessary vehicle maneuvers and stop and go traffic. ITS technologies are expected to provide positive impact on fuel economy for both trucks and passenger vehicles by controlling traffic more efficiently.

Current and past research on the development and evaluation of VSL, RM and LC control reported consistent improvements in traffic safety using theory, macroscopic model simulations and some field experiments (den Hoogen & Smulders, 1994; Lu & Shladover, 2014; Wang & Ioannou, 2011a). The impact of these control approaches to traffic mobility and environment has been controversial. Although most previous studies showed improvements in traffic mobility in macroscopic model simulations with different traffic flow control strategies, when it comes to microscopic simulations and field tests, these improvements are not consistent under different traffic conditions or incident scenarios. In some cases, the travel time is improved and in others deteriorated due to traffic flow control which raises questions as to the ability of VSL, RM and LC to improve traffic mobility (Baldi, Michailidis, Kosmatopoulos, Papachristodoulou, & Ioannou, 2014; Gao, 2012; Ioannou, Wang, Abadi, & Butakov, 2012; Kejun, Meiping, Jianlong, & Xiaoguang, 2008; Torne Santos, Rosas, & Soriguera, 2011). Most researchers attribute the inconsistencies in travel time and environmental impact improvements to the highly disordered and stochastic traffic conditions at congested bottlenecks, which are difficult to predict and regulate. The presence of trucks exacerbates the disordered condition (den Hoogen & Smulders, 1994; Ioannou et al., 2012; Torne Santos et al.,

2011; Wang & Ioannou, 2011a). While these arguments have an element of truth, the following questions need to be answered:

(1) Is it possible to reduce the disorder at the bottleneck, even with high volume of trucks, so that the consistency between macroscopic and microscopic model simulations can be improved?

(2) Is it possible to find efficient VSL, RM and LC control strategies which are able to improve the traffic mobility and the environment at highway bottlenecks and be robust with respect to different incident scenarios?

(3) Given the complexity of underlying causes of highway congestion, is it possible to integrate different control techniques to form a coordinated traffic flow control scheme that will improve overall performance?

The purpose of this work is to provide answers to the above questions. In particular a lane change controller which removes capacity drop at incidents and bottlenecks so that macroscopic models are consistent with microscopic model simulations in improving traffic flow characteristics is proposed and analyzed. The lane change (LC) controller is then combined with a variable speed limit (VSL) controller designed based on the cell transmission model using feedback linearization. In (Zhang & Ioannou, 2017a), stability analysis is performed for a combined VSL and LC controller. In(Zhang & Ioannou, 2017b), the controller is further integrated with the ramp metering (RM) controller. In this report, we demonstrate the complete analysis and design procedure of the integrated highway traffic flow controller. We analytically show that with the disturbance of the ramp flow, global stability can be guaranteed for a subsystem of the highway segment under consideration. The conditions under which the controller is feasible for implementation are also discussed. The integrated traffic flow controller is evaluated using a microscopic simulator based on the commercial software VISSIM ("VISSIM 5.30-04 User Manual," 2011). Simulation results show that the integrated controller is able to provide significant and consistent improvements in traffic mobility, safety and environmental impact.

System Modeling

Capacity Drop at Highway Bottleneck

For a highway segment, a bottleneck is the point with lowest flow capacity. The flow rate of the bottleneck determines the throughput of the entire highway segment. Therefore, the modeling of the bottleneck traffic flow is crucial to the design of an efficient traffic control strategy. A bottleneck can be introduced by lane drop, incident lane blockage, merge point or other road conditions.

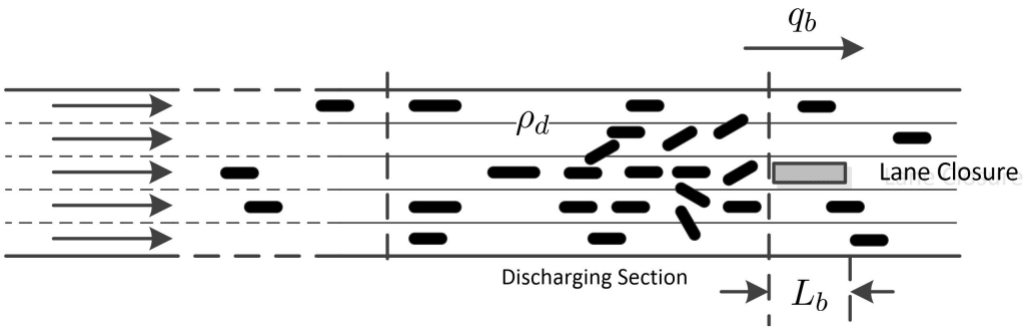

Figure 1. Highway Bottleneck

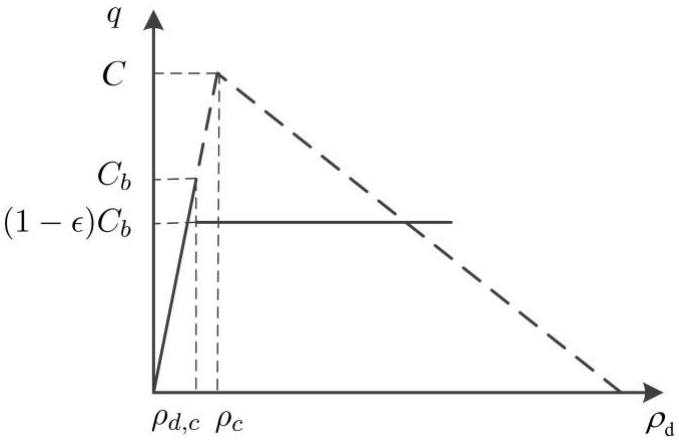

Figure 2. Fundamental Diagram of Highway Bottleneck

Figure 1 shows a highway segment with 5 lanes, to which a bottleneck is introduced by an incident that blocks one lane. The length of the bottleneck is denoted by L_b, which is assumed to be small enough that the effect of the density within L_b is negligible and will not affect the bottleneck flow. We assume that the capacity of the highway segment before the incident is C. Then the ideal capacity of the bottleneck after the incident should be $C_b = \frac{4}{5}C$. The flow rate q_b at the bottleneck is determined by ρ_d, the vehicle density of the immediate upstream section of the bottleneck, which is referred to as the discharging section in Figure 1. We assume a triangular fundamental diagram, that is, when the value of ρ_d is lower than the critical density $\rho_{d,c}$, $q_b = v_d\rho_d$, where v_d is the speed limit in the discharging section. Otherwise, a queue will form at the discharging section which propagates upstream as the demand of the bottleneck becomes higher than its capacity C_b. Forced lane changes performed by the vehicles in the queue reduce the speed of flow in the open lanes. Therefore, the capacity would drop to $C_b' = (1-\epsilon)C_b$ once the queue forms (Jin & Jin, 2015; Kontorinaki, Spiliopoulou, Roncoli, & Papageorgiou, 2016; Muralidharan & Horowitz, 2015) . Here ϵ denotes the intensity of capacity drop. The value of ϵ is related to the geometry of the bottleneck and characteristics of the traffic flow. The value of ϵ will get higher with the increase of the volume of trucks, due to the slow dynamics and large size of trucks. The relationship between ρ_d and q_b is shown as solid line in Figure 2 and is described by the equation

$$q_b = \begin{cases} v_d \rho_d, & \rho_d \le \rho_{d,c} \\ (1-\epsilon) C_b, & \rho_d > \rho_{d,c} \end{cases} \tag{1}$$

where $C_b = v_d \rho_{d,c}, \epsilon \in (0,1)$.

Cell Transmission Model of Highway Traffic

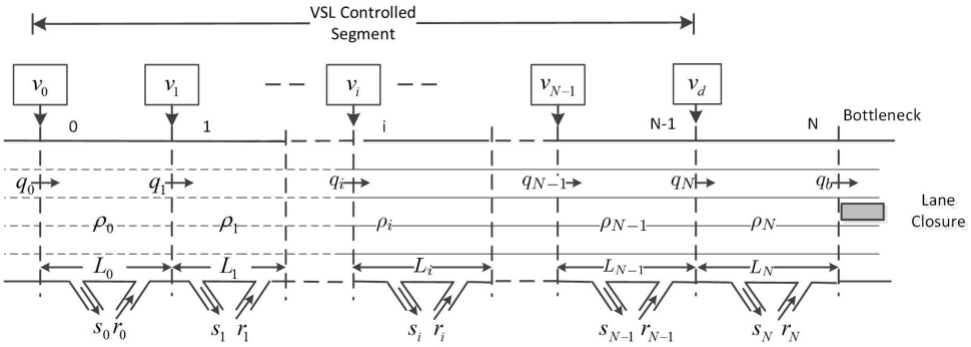

Figure 3. Configuration of VSL and RM Control System

The highway segment to be controlled by the integrated VSL and RM controller is shown in Figure 3. The bottleneck is introduced by a lane closure. The highway segment upstream the bottleneck is divided into $N+1$ sections, which are indexed as sections 0 through section N. For $i = 0, 1, \dots, N$, ρ_i, q_i, r_i, s_i represent the vehicle density, mainline in-flow rate, on-ramp flow rate and off-ramp flow rate in section i respectively, where ρ_i, s_i are measurable, r_i are determined by the RM controller, therefore also measurable. For $i = 0,1, \dots, N-1$, v_i denotes the variable speed limit in section i. The speed limit in section N, which functions as the discharging section in Figure 1, is constant and equals v_d. q_b denotes the flow rate through the bottleneck. Let L_i be the length of section i, for $i = 0,1, \dots, N$. According to the flow conservation law, we have

$$\begin{aligned} \dot{\rho}_i &= \frac{1}{L_i}(q_i - q_{i+1} + r_i - s_i), \qquad \text{for } i = 0, 1, \dots, N-1 \\ \dot{\rho}_N &= \frac{1}{L_N}(q_N - q_b + r_N - s_N) \end{aligned} \tag{2}$$

Under the assumption of triangular fundamental diagram, we have

$$\begin{aligned} q_0 &= \min\{d, C_0, w_0(\rho_{j,0} - \rho_0)\}, \\ q_i &= \min\{v_{i-1}\rho_{i-1}, C_i, w_i(\rho_{j,i} - \rho_i)\} \text{ , for } i = 1, 2, \dots, N \end{aligned} \tag{3}$$

where d is the demand flow of this highway segment and is assumed to be constant for the control time under consideration. $\rho_{j,i}$ is the jam density of section i, at which q_i is 0. w_i is the backward propagating wave speed in section i, C_i the capacity, i.e. the maximum possible flow rate in section i. $C_i = v_d \rho_{i,c}$, where $\rho_{i,c}$ is the critical density in section i.

The bottleneck flow q_b is given by equation (1), where ρ_d is replaced by ρ_N. We should note that C_N and $\rho_{N,c}$ are not the same as C_b and $\rho_{d,c}$. When ρ_N reaches $\rho_{d,c}$, q_b starts decreasing but section N still has enough space for vehicles in section $N-1$ to flow in. Therefore, $\rho_{N,c} > \rho_{d,c}, C_N > C_b$. The goal of the integrated traffic controller is to stabilize the system described in (1)-(3) and maximize the flow rate q_b. According to (1), maximum q_b is obtained at $\rho_N = \rho_{d,c}$, which is a discontinuity point in the fundamental diagram. From the macroscopic point of view, it is possible to maintain that $\rho_N = \rho_{d,c}$ with VSL controller alone (Jin & Jin, 2015). However, microscopic simulations in Zhang & Ioannou, 2017a demonstrate that when congestion occurs at the bottleneck, the queue accumulates so fast that VSL control can hardly reduce the density back to $\rho_{d,c}$, therefore it fails to maintain maximum flow. The reason is explained in the following subsection.

Effects of Lane Change Control

To study the effect of lane change control, we build a microscopic traffic simulation model using VISSIM for the traffic along the highway segment in Figure 1, which is 8 km long with 5 lanes. The bottleneck is formed by an incident which blocks the middle lane. We investigate the relationship between the bottleneck flow q_b and the density ρ_d in the 500 m long discharging section immediately upstream the bottleneck under different levels of traffic demand without any VSL and RM control. We consider two cases: In one case the drivers have no idea of the bottleneck or incident or that the lane they are in will be closed downstream and are forced to change lanes when the lane obstruction becomes visible. The other case is that the drivers are informed ahead of time that there is an upcoming obstacle and are asked to change lanes appropriately. How and when to inform the drivers upstream to change lanes is referred to as lane change (LC) control and its design will be presented in the following section.

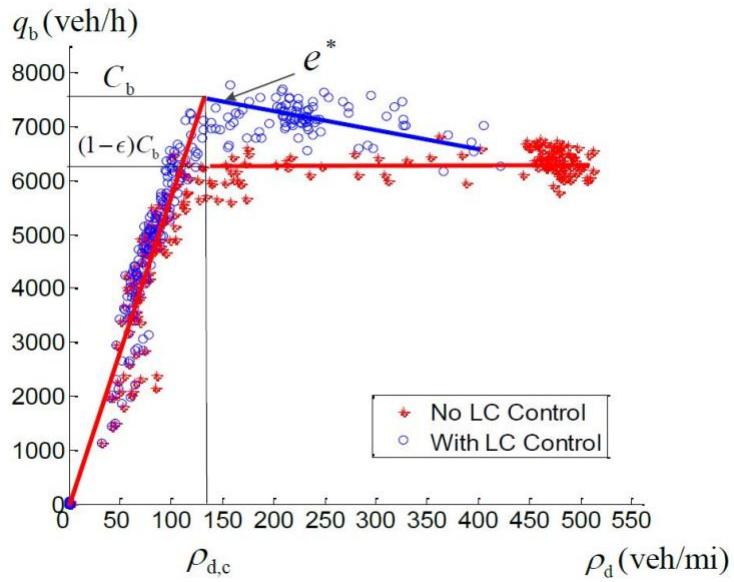

Figure 4. Fundamental Diagram with and without Lane Change Control

In Figure 4, the small blue circles describe the fundamental diagram in the case of lane change control. The red asterisks show the corresponding fundamental diagram in the absence of lane change control. We can see that when LC control is applied, the capacity of the bottleneck is around 7600 veh/h. However, when there is no LC control, q_b stops increasing even before it reaches the capacity. The highest flow rate is around 6300 veh/h. When vehicles approach the incident spot without being aware that their lane is blocked, they are forced to slow down considerably and change lanes. These forced lane changes at low speed cause the traffic to slow down in the open lanes leading to lower volume, while the average density of the discharging section, ρ_d, is still low. Other parts of the fundamental diagram in the no control case fit equation (1) very well. We can calibrate the parameters as, $\rho_{d,c} = 135$ veh/mi, C_b=7600 veh/h and ϵ = 0.16. The above microscopic traffic behavior of the bottleneck makes it difficult for VSL and RM control to increase q_b at the bottleneck, as VSL and RM are only able to regulate the average density ρ_d in the discharging section, but cannot eliminate the forced lane changes at the vicinity of the bottleneck.

On the other hand, with the LC control, we can see that

(1) no obvious capacity drop is observed at $\rho_d = \rho_{d,c}$.

(2) q_b at $\rho_d = \rho_{d,c}$ is approximately linear with a negative slope w_b, which represents the wave propagation rate.

(3) most data points scatter close to $\rho_d = \rho_{d,c}$. The points of high density are rare.

These observations show that the LC controller is able to reduce the number of vehicles stops in the queue at the bottleneck and decrease the vehicle density, which makes the system continuous at the critical point. As a consequence of the LC control action, in the cell transmission model the relationship between ρ_N and q_b can be modeled as:

$$q_b = \begin{cases} v_d \rho_N & \rho_N \leq \rho_{d,c} \\ w_b(\rho_{j,d} - \rho_N) & \rho_N > \rho_{d,c} \end{cases} \tag{4}$$

where $\rho_{j,d} = \frac{v_d \rho_{d,c}}{w_b} + \rho_{d,c}$.

Although the LC control is able to recover the triangular shape of the fundamental diagram, when the demand is higher than the capacity C_b, a congestion will still occur at the bottleneck. Now the goal is to design an integrated traffic flow controller to stabilize system (2)-(4) by homogenizing the densities in all sections and have them converge to an equilibrium which corresponds to the maximum possible flow as shown in the following section.

Integrated Variable Speed Limit, Ramp Metering and Lane Change Controller

In this section, an integrated variable speed limit, ramp metering and lane change controller is proposed. The goal is to maintain the bottleneck flow q_b at the maximum possible level and homogenize the traffic conditions in the overall controlled highway segment. We assume that the RM controller is already in place and develop the VSL to take into account and compensate

for the effects of RM. We consider the ALINEA/Q ramp metering strategy to manage the on-ramp flows and the queue lengths on the ramps.

Design of Lane Change Controller

The design of LC controller includes the pattern of the LC recommendation messages and the distance from the incident or bottleneck that the LC control recommendations are initiated. As we will explain below the control variable for LC control is the location of the LC recommendation which depends on a nonlinear spatial model that we developed.

Lane Change Recommendation Messages

Suppose a general highway segment has m lanes, with Lane 1 (Lane m) being the right (left) most lane in the direction of flow. We select the LC recommendation message S_i for lane i, i $= 1,2, \dots, m$ using the following rules:

(1) For $1 \leq i \leq m$, if lane i is open, $S_i =$ "Straight Ahead";

(2) For $i = 1$ $(i = m)$, if lane i is closed, $S_i =$ "Change to Left (Right)";

(3) For $1 < i < m$, if lane i is closed, lane $i - 1$ and lane $i + 1$ are both open, $S_i =$ "Change to Either Side";

(4) For $1 < i < m$, if lane i is closed, lane $i - 1$ (lane $i + 1$) is closed but lane $i + 1$ (lane $i - 1$) is open, $S_i =$ "Change to Left (Right)";

(5) For $1 < i < m$, if lane i is closed, lane $i - 1$ and lane $i + 1$ are both closed, then we check S_{i-1} and S_{i+1}. If $S_{i-1} = S_{i+1}$, then $S_i = S_{i-1} = S_{i+1}$, else if $S_{i-1} \neq S_{i+1}$, $S_i =$ "Change to Either Side".

Rules (1) -(5) determine the LC recommendation messages depending on the incident location. The 5 rules cover all incident cases and are also mutually disjoint. Therefore, they are well-defined and self-consistent.

Length of LC Control Segment

The control variables in the LC control are the length of the LC control segment and the location of the LC recommendations. A LC recommendation is given in each lane within the segment. The length of the LC controlled segment needs to be long enough in order to provide adequate space and time for upstream vehicles to change lanes. However, if the length is too long it may cause other problems as the blocked lane will appear empty thus inviting more lane changes in and out of the blocked lane which is going to deteriorate performance in terms of unnecessary maneuvers. Intuitively, if more lanes are closed at the bottleneck, a longer LC control distance is required. In addition, the capacity of the bottleneck and demand will also affect the LC control distance. We used extensive microscopic simulation studies to develop the following empirical model (5) that generates the length of the LC controlled section d_{LC} as:

$$d_{LC} = \xi \cdot n \tag{5}$$

where n is the number of lanes closed at the bottleneck, ξ a design parameter related to the capacity of bottleneck and the traffic demand which in our case is found to have the relationship shown in Figure 5. For a specific highway segment, the minimum value of ξ required under different traffic demands can be found by simulation. The model (5) is empirical and more spatial than temporal despite the dependence of ξ on demand which may be time-varying. The purpose of the LC control is to ask drivers to start changing lanes before the incident. It is an off and on controller i.e. change lanes or not required to change lanes. It is different than the VSL and RM controllers which are more dynamic.

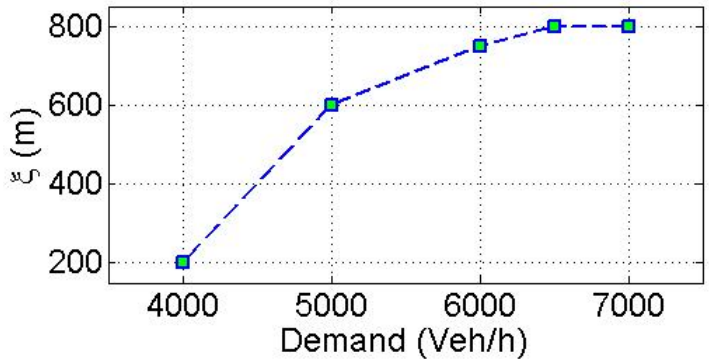

Figure 5. ξ under Different Traffic Conditions

Desired Equilibrium Point

We consider the demand $d > C_b$, which may introduce congestion at the bottleneck. The speed limit in section 0 needs to be lowered in order to suppress the traffic flow entering the downstream sections, therefore the density ρ_0 will increase. We want the equilibrium densities in the subsystem which contains section 1 through section N, $\rho_1^e, \rho_2^e, \dots, \rho_N^e$, to be homogenized and the bottleneck flow to be maximized. From the nonlinear system (2)-(4), we calculate the equilibrium point by setting the derivatives in (2) to zero. For section N, the density ρ_N needs to be maintained at the critical density $\rho_{d,c}$ thus the maximum flow rate is achieved. For section 1 through $N-1$, we set

$$\rho_1^e = \cdots = \rho_N^e = \rho_{d,c} \tag{6}$$

hence at the equilibrium point (6), the densities in section 1 through N would be the same and the upstream traffic flow of the bottleneck is homogenized. The corresponding VSL commands at the equilibrium point (6) are:

$$\begin{aligned} v_{0,ss} &= w_0 \frac{C_b - \sum_{j=1}^{N} R_j}{\rho_{j,0} + \sum_{j=1}^{N} R_j - C_b} \\ v_{i,ss} &= v_d - \sum_{j=i+1}^{N} R_j \,, i = 1,2,\dots,N-1 \end{aligned} \tag{7}$$

Where R_i is the net ramp flow in section i, i.e. $R_i = r_i - s_i$, for $i = 1,2,\dots,N$. Therefore, at equilibrium point (6), the VSL commands are functions of the ramp flows.

At this point, we consider the subsystem of (2)-(4) which contains section 1 through section N. The dynamics of ρ_0 will be analyzed in Lemma 1. The equilibrium point (6) is the desired equilibrium point which maximizes the flow at the bottleneck and homogenizes the upstream traffic when the demand exceeds the capacity of the bottleneck. The subsystem density dynamics of section 1 through N can be expressed as follows:

$$\dot{\rho}_i = \frac{1}{L_i}(v_{i-1}\rho_{i-1} - v_i\rho_i + R_i), i = 1,2,\dots,N-1$$

$$\dot{\rho}_N = \begin{cases} \frac{1}{L_n}(v_{N-1}\rho_{N-1} - v_d\rho_N + R_i), & \rho_N \le \rho_{d,c} \\ \frac{1}{L_N}\left[v_{N-1}\rho_{N-1} - w_b(\rho_{j,b} - \rho_N) + R_i\right], & \rho_N > \rho_{d,c} \end{cases} \quad (8)$$

In (8), the only switching point is $\rho_N = \rho_{d,c}$. This is consistent with real-world, since the capacities of upstream sections are much larger than C_b. As long as system (8) converges to the desired equilibrium point, the steady-state bottleneck flow is maximized and upstream traffic is homogenized.

Feedback Linearization VSL Controller

For the design and analysis of the VSL controller we define the deviations of the state of (8) from the desired equilibrium (6) by defining the error system as: $e_i = \rho_i - \rho_i^e$ for $i = 1,2,\dots,N$, which together with (8) gives us the following set of differential equations that describe the deviation of densities in each section from their desired equilibrium values.

$$\dot{e}_i = \frac{1}{L_i}(v_{i-1}\rho_{i-1} - v_i\rho_i + R_i), i = 1,2,\dots,N-1$$

$$\dot{e}_N = \begin{cases} \frac{1}{L_n}(v_{N-1}\rho_{N-1} - v_d\rho_N + R_i), & e_N \le 0 \\ \frac{1}{L_N}\left[v_{N-1}\rho_{N-1} - w_b(\rho_{j,b} - \rho_N) + R_i\right], & e_N > 0 \end{cases} \quad (9)$$

The problem is to select v_0 through v_N in order to stabilize system (9) and force all the errors to converge to zero.

We introduce the following feedback controller which cancels all nonlinearities and forces the closed-loop system to be linear with an approach known as feedback linearization(Khalil, 1996). We choose

$$v_i = \frac{-\lambda_i L_{i+1} e_{i+1} + v_d\rho_{d,c} - \sum_{j=i+1}^{N} R_j}{\rho_i}, i = 0,1,\dots,N-1 \quad (10)$$

$$v_{N-1} = \begin{cases} \dfrac{-\lambda_{N-1} L_N e_N + v_d \rho_N - R_N}{\rho_{N-1}}, & e_N \le 0 \\ \dfrac{-\lambda_{N-1} L_N e_N + w_b(\rho_{j,b} - \rho_N) - R_N}{\rho_{N-1}}, & e_N > 0 \end{cases}$$

Where $\lambda_i > 0$ for $i = 0,1,\dots,N-1$ are design parameters. With the feedback linearization controller (10), the closed-loop system becomes:

$$\begin{aligned} \dot{e}_i &= -\lambda_{i-1} e_i + \frac{L_{i+1}}{L_i} \lambda_i e_{i+1}, i = 1,2,\dots,N-2 \\ \dot{e}_{N-1} &= \begin{cases} -\lambda_{N-2} e_{N-1} + \dfrac{L_N}{L_{N-1}} (\lambda_{N-1} - v_d) e_N, & e_N \le 0 \\ -\lambda_{N-2} e_{N-1} + \dfrac{L_N}{L_{N-1}} (\lambda_{N-1} + w_b) e_N, & e_N > 0 \end{cases} \\ \dot{e}_N &= -\lambda_{N-1} e_N \end{aligned} \tag{11}$$

The stability properties of the closed-loop system (11) are described by the following Theorem.

Theorem 1. For a given demand $d > C_b$, the equilibrium point $e_i = 0$, for $i = 1,2,\dots,N$ is a unique, isolated equilibrium point of the closed-loop system (11) and is guaranteed to be globally exponentially stable. The rate of exponential convergence depends on the control design parameters $\lambda_i, i = 0,1,\dots,N-1$.

The proof of Theorem 1 can be found in Zhang & Ioannou, 2017c.

Observing the equations of controller (10), we can see that the VSL commands react to the ramp flows so that the effects of ramp flows are compensated and the densities are maintained at the desired values. Intuitively, if the demand from ramps is too high, the VSL controller will not be able to maintain the equilibrium point (6). The following lemma gives the condition of ramp flows under which the VSL controller (10) will fail.

Lemma 1. For each section $i = 0,1,\dots,N$, if the sum of the net ramp flows in all its downstream sections is higher than the bottleneck capacity, i.e. if $\sum_{j=i}^{N} R_j > C_b$, for all $i = 0,1,\dots N$, the feedback linearization VSL controller (10) is not feasible and will not be able to stabilize system (8) at equilibrium point (6).

The proof of Lemma 1 can be found in Zhang & Ioannou, 2017c.

Lemma 1 indicates that if the ramp flows exceed the downstream capacity , then the VSL controller (10) can no longer stabilize the system at equilibrium point (6) as the only flow it controls is the one entering the network from the main lanes. The feedback linearization controller compensates the ramp flows by reducing the mainline flow. If the sum of ramp flows equals to the bottleneck capacity, then the VSL controller needs to completely cut off the

mainline flow. Therefore, we need proper ramp metering controller to manage the ramp flows to keep the balance between the mainline flow and the ramp flows.

Selection of v_d

In model (8), v_d is the speed limit in the discharging section. The steady-state values of the VSL commands in controller (10) is $v_{i,ss} = v_d - \sum_{j=i}^{N} R_j / \rho_{d,c}$. Intuitively, we should set v_d at the highest possible value so that the speed limit along the controlled highway segment will be the highest which increases the flow rate. However, the microscopic simulation in Zhang & Ioannou, 2017a shows that when v_d is set to be the free flow speed v_f, the actual traffic flow at the bottleneck in microscopic simulations cannot follow this speed limit. We attribute this deviation to modeling error, speed limit following delay and the friction effect. This deviation of speed will not harm the benefit of VSL with respect to traffic mobility when designing the VSL controller based on the triangular fundamental diagram as long as ρ_d is stabilized at $\rho_{d,c}$. However, if the speed limit upstream the bottleneck is v_f, vehicles need to decelerate when approaching the bottleneck, which leads to shockwaves that propagate upstream.

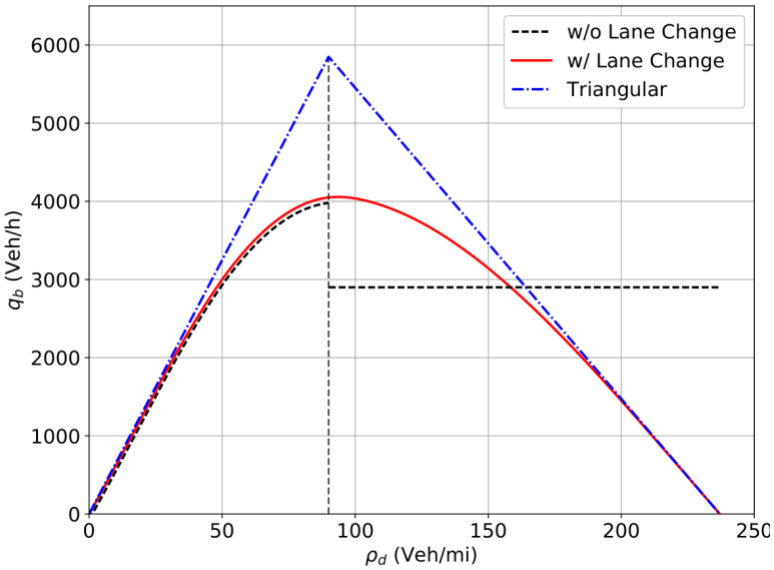

Figure 6. Fundamental Diagrams with and without LC

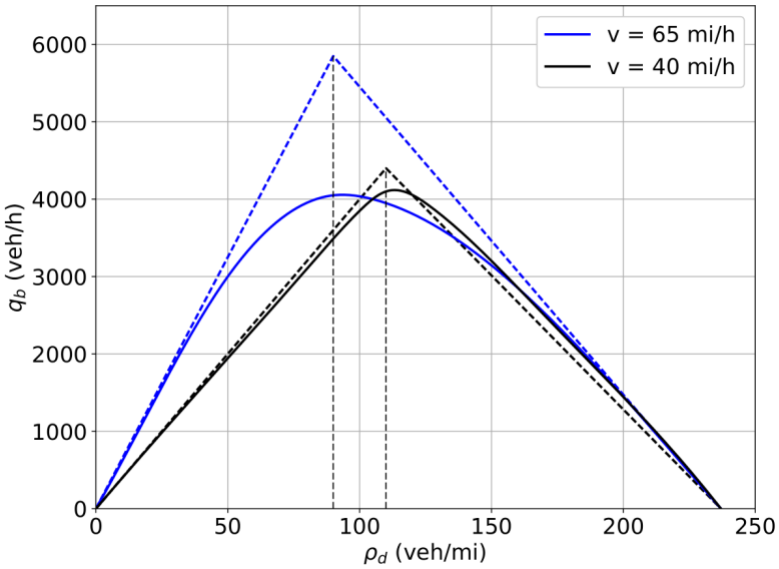

Figure 7. Fundamental Diagrams with and without VSL

If we decrease the speed limit upstream the bottleneck to v_d, such that $0 < v_d < v_f$, according to Papageorgiou, Kosmatopoulos, & Papamichail, 2008, the critical density in the fundamental diagram will be shifted to a higher value and the slope of the under-critical part of the fundamental diagram will be decreased and made closer to a straight line. Our microscopic simulations confirm this statement. The black solid line in Figure 7 shows the fundamental diagram under a speed limit of 40 mi/h. Compared to the one under 65 mi/h, which is shown as the blue solid line in Figure 7, the capacity of the bottleneck is not decreased despite the fact that under a lower speed limit the critical density is increased from $\tilde{\rho}_{d,c}$ to $\rho_{d,c}$. As we can see in the figure, this fundamental diagram is very close to its triangular approximation, that is, the speed deviation at $\rho_{d,c}$ is very small. If we design the integrated VSL and RM controller based on this fundamental diagram and let the VSL command converge to v_d at the equilibrium state, the shockwave upstream the bottleneck will be attenuated. We demonstrate this with microscopic simulations later in this report.

Constraints on VSL Commands

In the previous section, we showed that the feedback linearization controller (10) forces the closed-loop system (11) to be exponentially stable. However, it is not possible to follow speed limits which vary continuously with time as given in (10) due to practical considerations. For a practical VSL control we introduce the following constraints:

(1) *Discretization in time.* We discretized the continuous time VSL control commands using the sampling period T_c so that the VSL command is kept constant to its value at $t = kT_c$ till $t = (k+1)T_c$ where $k = 0,1,2, \ldots$.

(2) *Finite command space.* We use a quantization of 5 mi/h to truncate the generated VLS commands.

(3) *Saturation of Speed Limit Variations.* It is not desirable to decrease the speed limit too fast in both time and space. The decrease should be within some threshold $C_v > 0$ between successive control periods and highway sections. In addition, the VSL commands should never exceed the legal speed limit.

Using the above constraints, we modify the VSL control commands as follows. Let $u_i(k)$ denotes $v_i(t)$ computed by equation (10) at $t = kT_c$. We have,

$$\tilde{v}_i(k) = \max\{[v_i(k)]_5\ , \bar{v}_i(k-1) - C_v, \bar{v}_{i-1}(k) - C_v\} \tag{12}$$

$$\bar{v}_i(k) = \begin{cases} v_{\max}\ , & \text{if } \tilde{v}_i(k) > v_{\max} \\ v_{\min}\ , & \text{if } \tilde{v}_i(k) < v_{\min} \\ \tilde{v}_i(k), & \text{otherwise} \end{cases} \tag{13}$$

for $i = 0,1,\dots,N-1, k = 0,1,2,\dots$. In (12), $[\cdot]_5$ is the operator which rounds a real number to its closest multiples of 5.$\bar{v}(k)$ in (13) is the final constrained VSL command for section i at time $t = kT_c$. The above modifications will influence the ideal performance of the VSL controller described by Theorem 1. Such modifications are necessary for every control application (Carlson, Papamichail, & Papageorgiou, 2011; Lu, Varaiya, Horowitz, Su, & Shladover, 2010; Wang & Ioannou, 2011b) and the way to deal with possible deterioration from the ideal performance is to use the design parameters $\lambda_0, \lambda_1, \dots, \lambda_{N-1}$ to tune the system using intuition and practical considerations. The selection of the feedback gains $\lambda_0, \lambda_1, \dots, \lambda_{N-1}$ has to consider the trade-offs between stability and robustness with respect to modeling errors.

Design of the RM Controller

According to Theorem 1, the VSL controller (10) can stabilize the system and improve mobility as long as the net ramp flow is lower than the bottleneck capacity. It seems that RM control is unnecessary. However, if no RM is applied and large ramp flows flush into the mainline, the merging of ramp flows will severely disturb the mainline flow. Furthermore, when the net ramp flow is high, the VSL controller (10) will suppress the mainline flow in order to spare the capacity for the ramp flows. That is, without RM control, the ramp flow will always have priority which may harm the fairness between the ramp flows and the mainline flow, or even make the VSL controller infeasible. Furthermore, the RM controller should be able to manage the queue on the ramps so that the queues do not spill backward to the urban road network. We adopt the ALINEA/Q, which modifies the classic ALINEA ramp metering strategy with queue adjustment. The original ALINEA/Q method proposed in (Smaragdis & Papageorgiou, 2003) includes the downstream occupancy and the queue length in the feedback loop. In this report, to be consistent with the VSL controller, we use the downstream density instead of occupancy.

For an on-ramp i, two RM rates, $r_i^d(k)$ and $r_i^q(k)$, are decided respectively based on the downstream density and the queue length on the ramp at each time step $t = kT_c$. The final RM rate $r_i(k)$ is the maximum of the two. i.e.,

$$r_i^d(k) = r(k-1) + \beta_d[\rho_{d,c} - \rho_i(k)]$$
$$r_i^q(k) = \beta_q[w_i^r - w_i(k)] + d_i(k-1) \quad (14)$$
$$r_i(k) = \max\{r_i^d(k), r_i^q(k)\}$$

where $\rho_i(k)$ is the density in the highway section that connects to ramp i, $w_i(k)$ is the queue length on ramp i at time step k, $d_i(k-1)$ is the demand from ramp i within time step $k-1$, w_i^r is the reference queue length of ramp i. $r_i^d(k)$ is an integral feedback controller that regulates $\rho_i(k)$ to be close to $\rho_{d,c}$, which helps maintain the vehicle density on the mainline at the desired equilibrium value. $r_i^q(k)$ adjusts the RM rate in order to prevent the queue length from being too large, i.e. if $w_i(k)$ is larger than w_i^r, the RM rate will increase to discharge excessive vehicles in the queue and newly arrived vehicles. Since the final RM rate is the maximum of the two, the ramp flow will get priority to pass the bottleneck if the ramp queue is large, while the mainline flow will get priority if the vehicle density on the mainline is high. In this way, the ALINEA/Q strategy maintains the fairness between the ramp flows and the mainline flow and avoids the ramp queues from exceeding certain bounds.

Numerical Simulations

We evaluate the proposed controller on a segment of the I-710 freeway in California, United States (between I-105 and the Long Beach Port). As shown in Figure 8, the highway segment is divided into 8 sections, the VSL signs are deployed at the beginning of section 0 through 6. An incident blocks the middle lane at the end of section 7 and creates a bottleneck. 4 on-ramps, which are equipped with RM, and 5 off-ramps are connected to the highway segment. The lane change control is deployed at the beginning of section 7. The simulation network is calibrated with real world data from the PeMS system (California Department of Transportation, 2015). The incident occurs at 5 minutes after simulation starts, and lasts for 30 min. The capacity of the highway segment is 6800 veh/h without incident. During the incident, the ideal bottleneck capacity is about 4500 veh/h. We load the network with the real demand at 5pm on Monday, which is a peak hour. The mainline demand is 4500 veh/h, the on-ramp demand from upstream to downstream are 400 veh/h, 500 veh/h, 300 veh/h, 300 veh/h respectively.

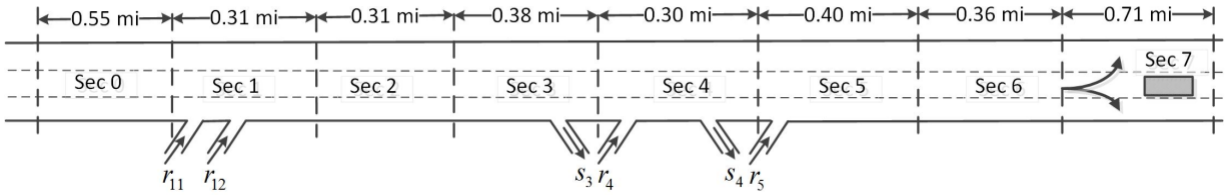

Figure 8. Geometry of Simulation Network

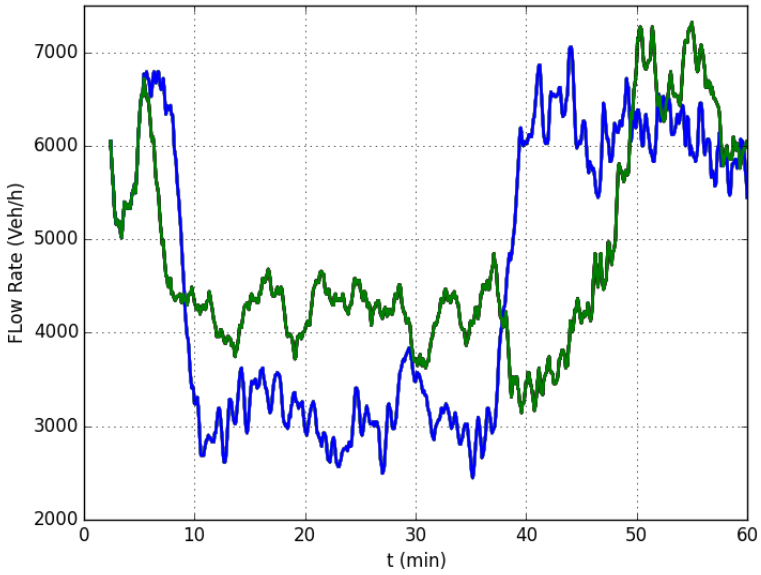

Figure 9. Bottleneck Flow — with control — without control

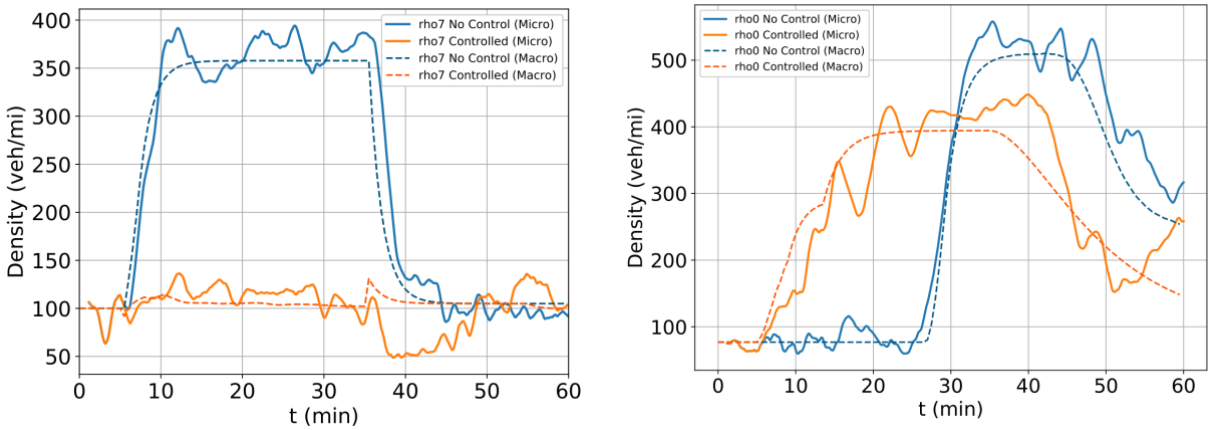

(a) Density in section 7 (b) Density in section 1

Figure 10. Vehicle Densities in Microscopic and Macroscopic Simulations

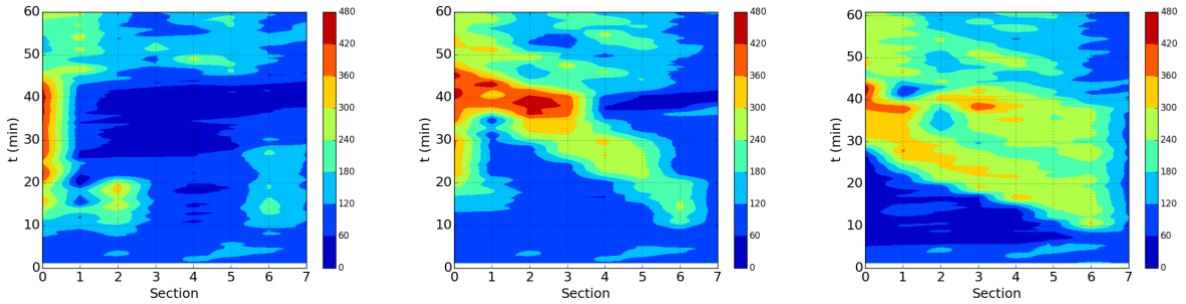

(a) $v_d = 40$ mi/h (b) $v_d = 65$ mi/h (c) No Control

Figure 11. Density Contours

Figure 9 shows the bottleneck flow with and without the integrated VSL, RM and lane change control. When there is no control, the flow rate decreases immediately to around 3000 veh/h due to the lane blockage and capacity drop, and increases right away after the incident is removed as the queue in the bottleneck area flushes downstream. When the controller is applied, the flow rate decreases to around 4200 veh/h, which is higher than that in the no control case since the capacity drop is avoided by the lane change control and VSL stabilizes the vehicle densities. The bottleneck flow starts increasing about 10 min after the incident is removed as the high-density area is held in section 0 by the VSL controller. The high-density wave moves forward from section 0 and the flow rate q_b starts increasing once the wave front reaches the bottleneck.

Figure 10 shows the curves of ρ_7 and ρ_0, which are the vehicle density of the discharging section and the first VSL controlled section, respectively. The solid lines are the microscopic simulation results, while the dashed lines show what is predicted by the macroscopic model. The simulation results are consistent between microscopic and macroscopic simulations. When there is no control, ρ_7 starts increasing immediately as the incident occurs at $t = 5$ min. In addition, the shockwave propagates upstream, which makes ρ_0 starts increasing at $t = 25$ min and reaches 500 veh/mi. The high density in section 0 does not discharge until 15 min after the incident is removed. When the integrated controller is applied, ρ_7 increases slightly and is stabilized at 110 veh/mi. ρ_0 increases immediately after the incident since v_0 decreases to reduce the flow into downstream sections and is stabilized at around 400 veh/h which is lower than that without control.

Figure 11 demonstrates the contour plot of vehicle densities with respect to time and space with different values of v_d. When $v_d = 40$ mi/h, high density is held in section 0 during the incident, while downstream sections are highly homogenized. ρ_2 is higher than $\rho_{d,c}$ at the beginning of the incident as the ramp flows r_{11} and ρ_{12} flush in but then discharged under control. The density in section 6 is slightly higher than $\rho_{d,c}$ as vehicles receive the lane change recommendations and make lane changes thus slightly disturbs the upstream flow. When $v_d = 65$ mi/h, as explained before, a shockwave propagates upstream. After the incident is removed, the vehicles in section 0 flush downstream and meet with the shockwave, which leads to a

high-density area in section 2. However, in this case, the discharging section is still well protected. As the shockwave propagates upstream, vehicle densities converge to $\rho_{d,c}$ gradually from downstream section to upstream section. This is because we use the cascade structure of VSL controller in Figure 3, which attenuates the shockwave section by section. Thus, the controller is robust to parameter selection. When there is no control applied, congestion occurs at the bottleneck after the incident. A shockwave moves backward and does not discharge until the incident is removed.

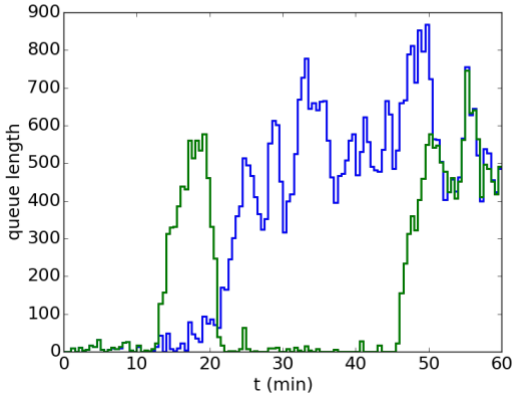

(a) Queue length on r_{11}

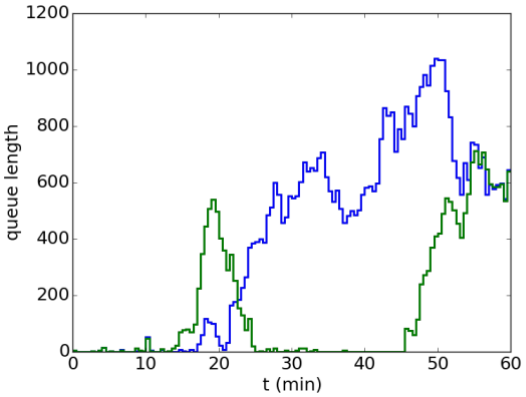

(b) Queue length on r_{12}

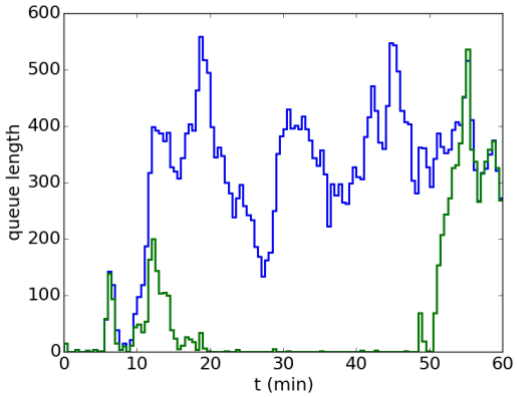

(c) Queue length on r_4

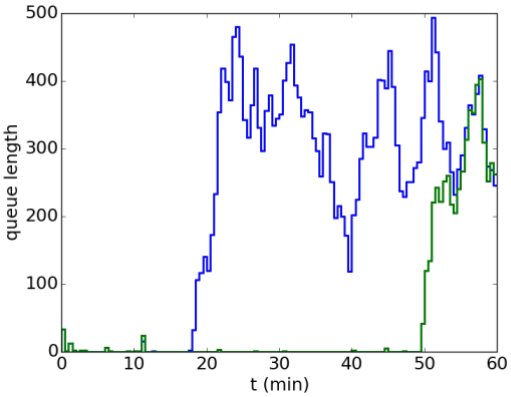

(d) Queue length on r_5

Figure 12. Queue Length with and without Control —VSL + RM, —RM only

Figure 12 shows the queue length on the four ramps in highway segment under consideration, with RM control alone and with the integrated controller. With RM control alone, the queues pile up fast as the densities in mainline increase. Due to the queue adjustment mechanism of ALINEA/Q, the queue lengths are maintained around the reference value. With the integrated controller, the queue lengths increase in the transient process when the incident begins, and the mainline density is being adjusted to the desired level and then discharge fast. After the

incident is removed, large flow flushes downstream, the RM controller decreases the rate to give priority to the mainline, therefore the queue lengths increase.

We use the following measurements to evaluate the performance of the proposed controller. The measurements start at the time instant that the incident begins ($t = 5$ min) and terminate at the time instant 10 minutes after the incident ends ($t = 45$ min), so that the traffic states can achieve steady-state. We collect the data of all vehicles that pass through the bottleneck during the above defined measuring periods and calculate the following values:

(a) Average travel time

$$\bar{T}_t = \sum_{i=1}^{N_v} (t_{i,out} - t_{i,in})/N_v$$

where $t_{i,in}$ and $t_{i,out}$ denote the time instant vehicle i enters and exits the network respectively. Note that our simulation network has enough space upstream of the controlled segment, therefore the time waiting in the queue is also counted.

(b) average number of stops ($\bar{s}$) and average number of lane changes ($\bar{c}$). Fewer stops and lane changes indicate smoother traffic flow and lower probability of crash, therefore better traffic safety (Ioannou et al., 2012).

$$\bar{s} = \sum_{i=1}^{N_v} s_i/N_v \ , \bar{c} = \sum_{i=1}^{N_v} c_i/N_v$$

where s_i, c_i are number of stops and lane changes performed by vehicle i respectively.

(c) average fuel consumption rate and average emission rates of CO2. These rates are uniformly defined as:

$$R = \sum_{i=1}^{N_v} E_i \ / \sum_{i=1}^{N_v} d_i$$

where E_i denotes the fuel consumed or a certain type of emission generated by vehicle i in the highway network, d_i represents the distance traveled by vehicle i in the network, and R denotes the fuel consumption rate or the tailpipe emission rate of CO2. The fuel consumption rate and emission rates are calculated using the MOVES model of the Environment Protection Agency (EPA) based on the speed and acceleration profile of each vehicle (EPA, 2014).

Table 1. Evaluation Results

Control Type	No Control	RM	VSL + LC	RM + VSL + LC	Improvement
T_t (min)	15.7	14.8	12.0	11.4	27%
$\bar{s}$	23.3	23.9	4.2	4.2	82%
$\bar{c}$	5.1	5.0	4.8	4.6	10%
CO2 (g/veh/mi)	585	580	548	538	8%
Fuel (g/veh/mi)	187	184	175	172	8%

Table 1 shows the evaluation results when there is no control, RM control only, VSL + LC only and RM+VSL+LC. When the integrated VSL, RM and LC controller is applied, the improvement in traffic mobility, safety and the environment is significant. The average travel time is reduced by about 27% as the bottleneck throughput is increased. For traffic safety, the number of stops dramatically decreased by 81% as the lane change control prevented vehicles from stopping at the bottleneck and waiting for lane changes. The 10% reduction in number of lane changes is contributed by both homogenization of mainline flow and the regulated merging behavior of ramp flows. For the environment metrics, the reductions of CO2 emission and energy consumption are usually proportional to each other, which are both around 8% in this case.

From Table 1, we can see that most improvement in traffic mobility is contributed by the VSL+LC controller. The RM controller can also improve the traffic mobility as well as the environment slightly as it attenuates the disturbance introduced by the ramp flow. However, the RM controller cannot reduce the number of stops and numbers of lane changes.

Conclusion

In this report, we first showed that forced lane change at the vicinity of the bottleneck is the major cause of the capacity drop phenomenon. We proposed a lane change controller which provides lane change recommendations to upstream vehicles in order to reduce or avoid capacity drop. An integrated variable speed limit, ramp metering and lane change controller for highway traffic flow is designed to improve mobility, safety and environmental impact at highway bottleneck and manage the queue lengths on the ramps. The integrated traffic flow controller guarantees global exponential convergence to the desired equilibrium point at which maximum possible flow rate is achieved. Microscopic VISSIM based simulations for a large segment of I-710 where the volume of trucks is relatively high are used to demonstrate the results and show consistent improvement in terms of traffic mobility and environmental impact.

Chapter 2: Comparison of Feedback Linearization and Model Predictive Techniques for Variable Speed Limit Control

Introduction

In Chapter 1, we developed an integrated VSL, RM and LC traffic flow controller, which guarantees stability of traffic flow, improves traffic mobility and safety while reducing the level of emission and fuel consumption. In this controller, the VSL control is developed using feedback linearization (FL) while in many similar studies published in literature model predictive control (MPC) appears to be the dominant approach. In this Chapter we compare the MPC with our FL approach in terms of performance, robustness and computational burden.

MPC is a widely studied control strategy in the development of VSL control. MPC based VSL control strategies compute the VSL commands by predicting the system behavior with dynamic models and solving finite-horizon optimal control problems at each time step in a receding horizon manner. Muralidharan et al. proposed a MPC VSL controller based on the link-node cell transmission model (LN-CTM) that is able to recover the bottleneck from capacity drop and obtain an optimal trajectory in the absence of capacity drop (Muralidharan & Horowitz, 2015). In 2014, Frejo et al. proposed a hybrid MPC controller which combines VSL with ramp metering. The proposed method reduced the computation load of the receding horizon optimization by using genetic and exhaustive algorithms while achieving a good performance in simulation (Frejo, Núñez, De Schutter, & Camacho, 2014). In (Zegeye, De Schutter, Hellendoorn, & Breunesse, 2009), an MPC VSL strategy was proposed using a car-following model to reduce both total time spent (TTS) and total emissions. It is shown that a reduction of TTS alone may not reduce the total emissions. In (Khondaker & Kattan, 2015), an MPC-based VSL controller was proposed to improve traffic safety, mobility and the environmental impact simultaneously in a connected vehicle context. In (Han et al., 2017), a MPC method is proposed based on a discrete first order model which takes into consideration the jam wave propagation.

Intuitively, since MPC control follows an optimization-based routine, it should provide the "optimal" performance to some extent. However, FL controller guarantees exponential convergence to an equilibrium point which corresponds to the highest bottleneck flow rate. Such a result is not proven analytically by using MPC.

In this chapter, we propose FL and MPC schemes for VSL-actuated highway traffic, where we assume that an LC controller is active upstream of the bottleneck. Both controllers are designed with a CTM-based model representing the ideal system. TTS performance and robustness with respect to perturbations on model parameters and measurement noise of the proposed controllers are evaluated via simulation studies. Results show both VSL controllers are able to improve the TTS under different levels of perturbation and measurement noise. However, feedback linearization-based VSL provides better performance than model predictive VSL with much less computational effort.

Nonlinear Model Predictive Control

Since we are comparing the performance of FL and MPC based VSL controller, for the sake of simplicity, we assume in system (8), all ramp flows equal 0, i.e. $R_i = 0$. According to equation (7), the steady state values of the VSL commands become the following:

$$v_{0,ss} = w_0 \frac{C_b}{\rho_{j,0} - C_b}$$
$$v_{i,ss} = v_d, i = 1,2, \dots, N-1 \quad (15)$$

Let $u_i(t) = v_i(t) - v_{i,ss}, i = 0,1, \dots, N-1, e = [e_1, e_2, \dots, e_N]^T$ and $u = [u_0, u_1, \dots, u_{N-1}]^T$. System (9) can be expressed implicitly as

$$\dot{e} = f(e, u)$$

We formulate the problem of finding the VSL commands $u_i(\cdot)$ that try to maintain system (8) at the equilibrium point by solving the following finite-horizon constrained optimal control problem (OCP):

$$\min_{u(\cdot)} \int_{kT_c}^{kT_c+T_p} e(\tau)^T \tilde{Q} e(\tau) + u(\tau)^T \tilde{R} u(\tau)\, d\tau$$
$$\text{s.t.} \quad e(kT_c) = \hat{e}(kT_c)$$
$$\forall \tau \in [t, t+T_p]:$$
$$\dot{e} = f(e, u)$$
$$v_{\min} - v_{i,ss} \leq u_i(\tau) \leq v_{\max} - v_{i,ss}, i = 0,1, \dots, N-1 \quad (16)$$

Where t is the current control sampling instant in time, $\hat{e}(t)$ is the measured state error taken at time t, $\tilde{Q}$ and $\tilde{R}$ are weighting matrices on error and control input, respectively, whereas T_P is the prediction horizon. The optimization problem is solved at the beginning of each control step kT_c, with $\hat{e}(kT_c)$as the initial condition. Constraint (13) has already been included in the constraints of the optimization problem. Constraint (12) is also applied to the MPC VSL commands before applied to the system.

Due to the continuous-time dynamics, the OCP (16) is an infinite dimensional optimization problem. We resort to approximating it as a finite dimensional nonlinear program (NLP) via the direct multiple shooting method (Bock & Plitt, 1984). Details on direct methods from numerical optimal control literature can be found in (Diehl, Bock, Diedam, & Wieber, 2006).

Numerical Simulation

Scenario setup

In this section, macroscopic simulations are used to evaluate the performance and robustness of the FL and MPC schemes combined with LC control on the I-710 network in Figure 8. Since we shut down all ramps the desired equilibrium point of this network is calibrated to be:

$$\rho_1^e = \rho_2^e = \cdots = \rho_7^e = 110 \text{ veh/mi}$$
$$v_{0,ss} = 15.8 \text{ mi/h}, v_{1,ss} = v_{2,ss} = \cdots = v_{6,ss} = 40 \text{ mi/h}$$

For the FL controller, we choose $\lambda_i = 50$, for $i = 0,1,\ldots,6$. The MPC controller is implemented using the direct multiple shooting method via the CasADi toolbox (Andersson, 2013) in MATLAB 8.5.0 (R2015a), on a 64-bit Windows PC with 3.4-GHz Intel Core i7 processor and 8-GB RAM, where IPOPT (Wächter & Biegler, 2006) is used for solving the NLPs. In our simulation, we choose the prediction horizon $T_p = 10$ min, which is much greater than the control time step $T_c = 30$ s. Weight matrices are chosen as $\tilde{Q} = \boldsymbol{I}$ and $\tilde{R} = 0.1\boldsymbol{I}$, with $\boldsymbol{I}$ denoting the identity matrix of appropriate dimensions. The feedback gain for FL and the prediction horizon T_p for MPC is tuned so that best performance in terms of total time spent is achieved for both controllers. Specifically, for MPC, together with the increase of T_p, the closed-loop performance is improved but the computation time is also increased. When $T_p \geq 10$ min, the closed loop performance will not improve with T_p. With $T_p = 10$ min, the computation time of MPC is around 0.35 seconds, whereas it is negligible for FL. The MPC scheme is still computationally tractable, as its computation time of 0.35 s per step is negligible with respect to the control time step of 30 s.

Performance and Robustness Analysis

To compare the performance and robustness of the FL and MPC VSL controllers, we evaluate the following criteria for the two controllers:

(1) Total time spent (TTS) which is defined as:

$$\text{TTS} = \int_0^T Q(t) + \sum_{i=0}^{N} \rho_i(t) L_i \, dt$$

where Q is the size of the queue upstream section 0, which is used to track the wait time of vehicles blocked outside the controlled segment and given by the following differential equation:

$$\dot{Q} = d - q_0, Q(0) = 0$$

and sensitivity of TTS with respect to

(2) perturbation on traffic demand,

(3) perturbation on model parameters and

(4) measurement noise.

The FL and MPC controllers are designed based on the ideal model (9), but the control commands are applied to the simulation model which with uncertainties. The structure of the simulation system is shown in Figure 13. For the traffic demand, we add up to ±20% perturbation on the nominal demand 6000 veh/h. For the model parameters, as shown in Figure 14, we respectively add up to ±20% perturbation on the nominal value of $\rho_{d,c}$ and C_b, which directly alter the shape of the fundamental diagram of the bottleneck section. For the

measurement noise, we use Gaussian white noise with different levels of standard deviation up to $\sigma = 0.1\rho_{d,c}$ to match the scale of the density measurements.

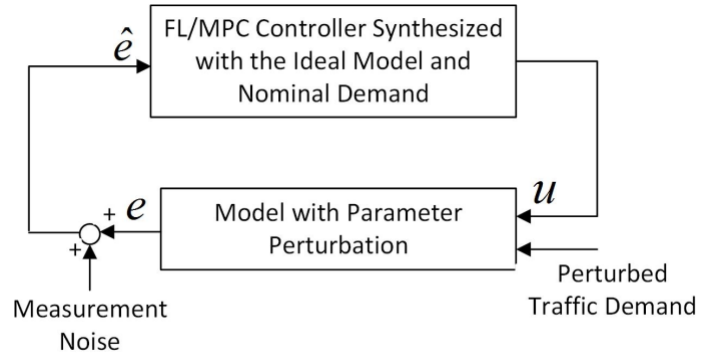

Figure 13. Simulation System

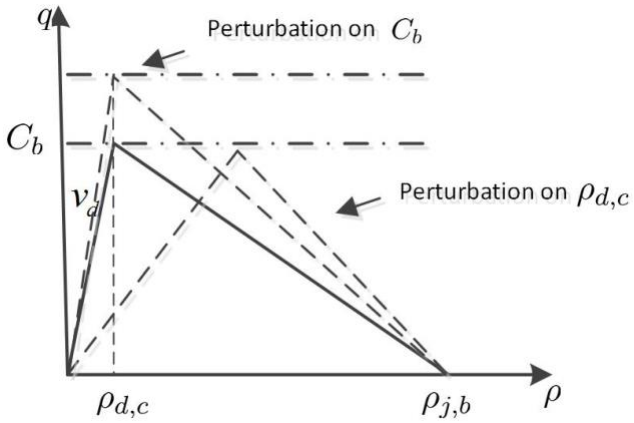

Figure 14. Parameter Perturbations

Figure 15 shows the behavior of the vehicle density in the discharging section under FL and MPC controller. Both controllers are able to maintain the density around the desired value ρ_7^e=110 veh/h after the incident occurs at $t = 5$ min. The oscillation is introduced by the roundup-to-5 constraint. However, the MPC controller introduces higher frequency chattering and a sharp decrease at the beginning of the incident.

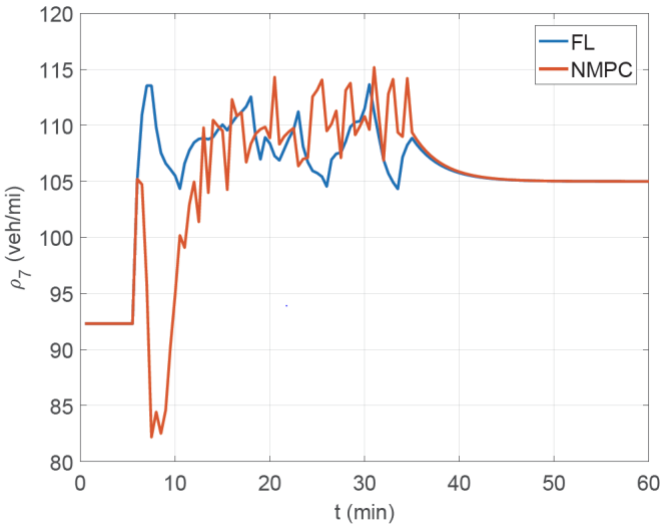

Figure 15. ρ_7 with FL and MPC

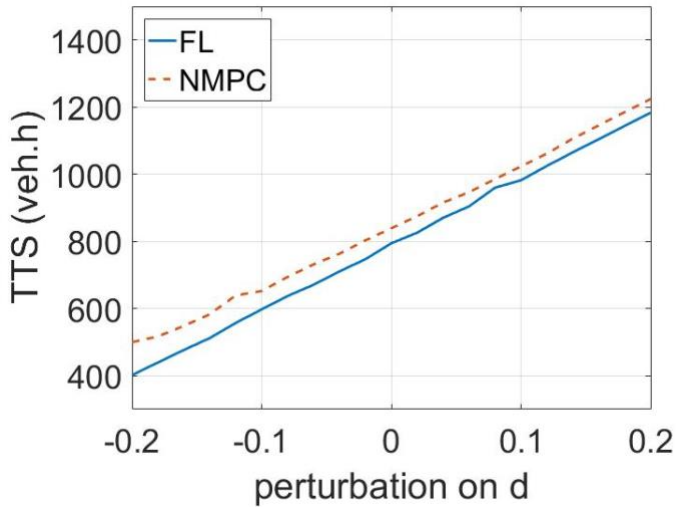

Figure 16. TTS of FL and MPC under perturbations on d

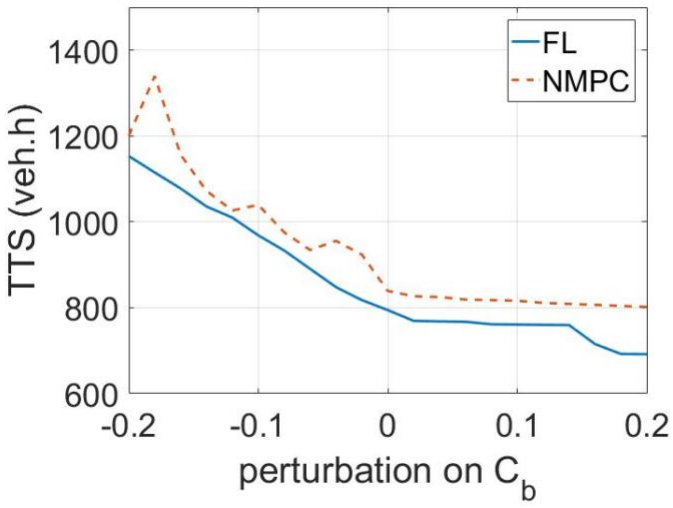

Figure 17. TTS of FL and MPC under perturbations on C_b

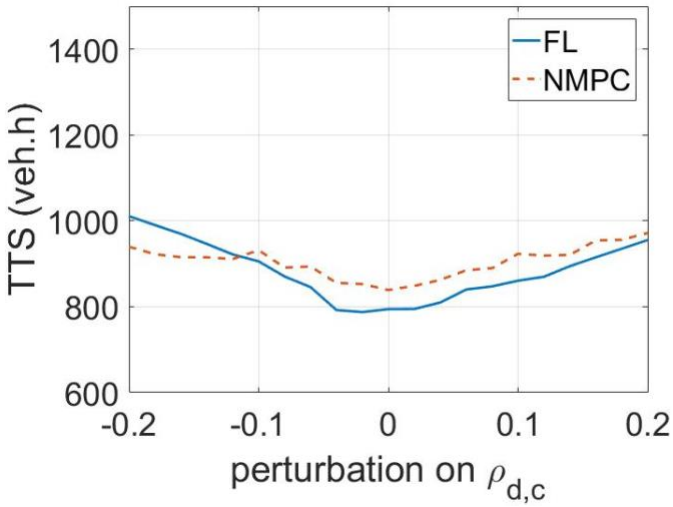

Figure 18. TTS of FL and MPC under perturbations on $\rho_{d,c}$

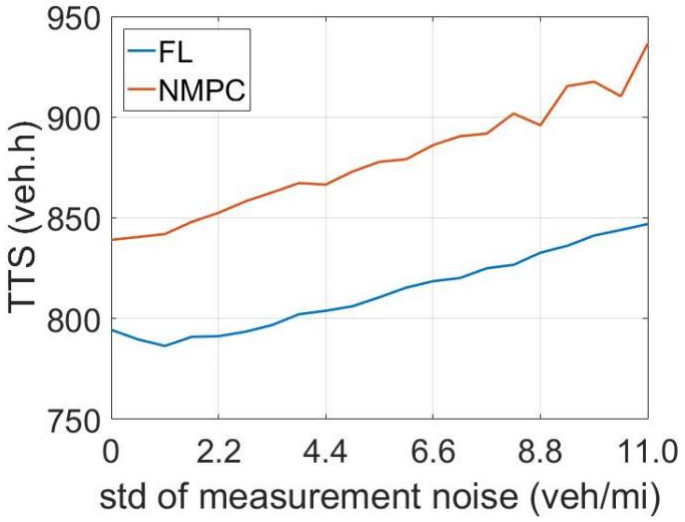

Figure 19. TTS of FL and MPC under measurement noise

A series of simulation experiments are conducted with different levels of perturbation and measurement noise. Figure 16 shows how TTS varies with varying demand levels. The figure shows that both controllers are able to function properly under various levels of demand and the TTS increases and decreases approximately linearly with the demand. This demonstrates that both MPC and FL VSL controllers are robust with respect to the variation of demand, which is due to the selection of the desired equilibrium point. At the equilibrium point, the speed limit in section 0 is decreased to block excessive traffic demand at upstream of the entire control segment, therefore the bottleneck flow is not affected. Furthermore, under different levels of perturbation, the performance of FL and MPC controllers is similar. But the TTS of FL is always slightly lower than that of MPC, which shows that MPC fails to beat FL in TTS although the control commands are generated by solving the optimization problem in receding horizon fashion.

In Figure 17 and Figure 18, the change in TTS is plotted with respect to different values of perturbations in the values of C_b and $\rho_{d,c}$, respectively. These results show that both controllers achieve significant improvements over the no control case and are able to operate properly even under situations with high amount of uncertainty in these model parameters. Due to perturbation in the values of C_b, the TTS under FL and MPC is increased by 45% and 43% in the worst case, respectively. Considering the fact that in this case the bottleneck capacity is decreased by 20% as a baseline, the TTS does not increase too much due to the modeling error. For perturbations in the value $\rho_{d,c}$ the FL is 27% worse and the MPC 16% worse when compared with the zero perturbations case.

The sensitivity of TTS performance in the case of varying levels of standard deviation in measurement noise is given in Figure 19, which shows that the TTS under both controllers increases with the standard deviation of measurement noise. The performance of FL is always better than that of MPC in this case.

Although the MPC controller is built based on an optimization scheme, it only achieves optimality over each prediction horizon instead of the entire control period. Furthermore, the FL controller guarantees global exponential convergence, while the stability and convergence properties of the MPC controller are yet to be established analytically.

Conclusion

In this chapter, we compared the properties of our FL integrated LC, VSL controllers with the corresponding MPC schemes proposed in literature. Using the total time spent as performance criterion, we evaluated and compared the performance and robustness with respect to perturbations on traffic demand, model parameters and measurement noise of the two controllers. Simulation results show that both controllers work properly under different levels of perturbation and measurement noise. Although the synthesis of MPC controller involves an optimal control routine and is computationally much more expensive, it does not provide better performance than the feedback linearization. In addition, it shows worse performance when it comes to robustness with respect to measurement noise.

References

Andersson, J. (2013, October). *A General-Purpose Software Framework for Dynamic Optimization*. Arenberg Doctoral School, KU Leuven, Department of Electrical Engineering (ESAT/SCD) and Optimization in Engineering Center, Kasteelpark Arenberg 10, 3001-Heverlee, Belgium.

Baldi, S., Michailidis, I., Kosmatopoulos, E. B., Papachristodoulou, A., & Ioannou, P. A. (2014). Convex Design Control for Practical Nonlinear Systems. *IEEE Transactions on Automatic Control*, *59*(7), 1692–1705. https://doi.org/10.1109/TAC.2014.2309271

Bock, H. G., & Plitt, K.-J. (1984). A multiple shooting algorithm for direct solution of optimal control problems. In *Proceedings of the IFAC World Congress*.

California Department of Transportation. (2015). Caltrans Performance Measurement System ({PeMS}). Retrieved from http://pems.dot.ca.gov/

Carlson, R. C., Papamichail, I., & Papageorgiou, M. (2011). Local feedback-based mainstream traffic flow control on motorways using variable speed limits. *IEEE Transactions on Intelligent Transportation Systems*, *12*(4), 1261–1276.

den Hoogen, E., & Smulders, S. (1994). Control by variable speed signs: results of the Dutch experiment. In *Road Traffic Monitoring and Control, 1994., Seventh International Conference on* (pp. 145–149).

Diehl, M., Bock, H. G., Diedam, H., & Wieber, P.-B. (2006). Fast direct multiple shooting algorithms for optimal robot control. In *Fast motions in biomechanics and robotics* (pp. 65–93). Springer.

EPA. (2014). Motor Vehicle Emission Simulator (MOVES) User Guide. *US Environmental Protection Agency*.

Frejo, J. R. D., Núñez, A., De Schutter, B., & Camacho, E. F. (2014). Hybrid model predictive control for freeway traffic using discrete speed limit signals. *Transportation Research Part C: Emerging Technologies*, *46*, 309–325.

Gao, K. (2012). *Multi-objective Traffic Management for Livability*. MS thesis, TU Delft, Delft, The Netherlands.

Han, Y., Hegyi, A., Yuan, Y., Hoogendoorn, S., Papageorgiou, M., & Roncoli, C. (2017). Resolving freeway jam waves by discrete first-order model-based predictive control of variable speed limits. *Transportation Research Part C: Emerging Technologies*, *77*, 405–420.

Ioannou, P., Wang, Y., Abadi, A., & Butakov, V. (2012). *Dynamic Variable Speed Limit Control: Design, Analysis and Benefits*.

Jin, H.-Y., & Jin, W.-L. (2015). Control of a lane-drop bottleneck through variable speed limits. *Transportation Research Part C: Emerging Technologies*, *58*, 568–584.

Kejun, L., Meiping, Y., Jianlong, Z., & Xiaoguang, Y. (2008). Model predictive control for variable speed limit in freeway work zone. In *Control Conference, 2008. CCC 2008. 27th Chinese* (pp. 488–493).

Khalil, H. K. (1996). Nonlinear Systems. *Prentice-Hall, New Jersey*, *2*(5), 1–5.

Khondaker, B., & Kattan, L. (2015). Variable speed limit: A microscopic analysis in a connected vehicle environment. *Transportation Research Part C: Emerging Technologies*, *58*, 146–159.

Kontorinaki, M., Spiliopoulou, A., Roncoli, C., & Papageorgiou, M. (2016). *Capacity drop in first-order traffic flow models: Overview and real-data validation*.

Lu, X.-Y., & Shladover, S. E. (2014). Review of Variable Speed Limits and Advisories. *Transportation Research Record: Journal of the Transportation Research Board*, *2423*(1), 15–23.

Lu, X.-Y., Varaiya, P., Horowitz, R., Su, D., & Shladover, S. (2011). Novel freeway traffic control with variable speed limit and coordinated ramp metering. *Transportation Research Record: Journal of the Transportation Research Board*, (2229), 55–65.

Lu, X.-Y., Varaiya, P., Horowitz, R., Su, D., & Shladover, S. E. (2010). A new approach for combined freeway variable speed limits and coordinated ramp metering. In *Intelligent Transportation Systems (ITSC), 2010 13th International IEEE Conference on* (pp. 491–498).

Muralidharan, A., & Horowitz, R. (2015). Computationally efficient model predictive control of freeway networks. *Transportation Research Part C: Emerging Technologies*, *58*, 532–553.

Papageorgiou, M., Hadj-Salem, H., & Middelham, F. (1997). ALINEA local ramp metering: Summary of field results. *Transportation Research Record: Journal of the Transportation Research Board*, (1603), 90–98.

Papageorgiou, M., Kosmatopoulos, E., & Papamichail, I. (2008). Effects of variable speed limits on motorway traffic flow. *Transportation Research Record: Journal of the Transportation Research Board*, (2047), 37–48.

Smaragdis, E., & Papageorgiou, M. (2003). Series of new local ramp metering strategies. *Transportation Research Record: Journal of the Transportation Research Board*, (1856), 74–86.

Torne Santos, J. M., Rosas, D., & Soriguera, F. (2011). Evaluation of speed limit management on C-32 highway access to Barcelona. In *Transportation Research Board 90th Annual Meeting*.

VISSIM 5.30-04 User Manual. (2011, February). Karlsruhe, Germany.

Wächter, A., & Biegler, L. T. (2006). On the implementation of an interior-point filter line-search algorithm for large-scale nonlinear programming. *Mathematical Programming*, *106*(1), 25–57.

Wang, Y., & Ioannou, P. (2011a). *Dynamic Variable Speed Limit Control: Design, Analysis and Benefits*. University of Southern California.

Wang, Y., & Ioannou, P. (2011b). New model for variable speed limits. *Transportation Research Record: Journal of the Transportation Research Board*, (2249), 38–43.

Zegeye, S. K., De Schutter, B., Hellendoorn, H., & Breunesse, E. (2009). Reduction of travel times and traffic emissions using model predictive control. In *American Control Conference, 2009. ACC'09.* (pp. 5392–5397).

Zhang, Y., & Ioannou, P. A. (2017a). Combined Variable Speed Limit and Lane Change Control for Highway Traffic. *IEEE Transactions on Intelligent Transportation Systems*, *18*(7), 1812–1823.

Zhang, Y., & Ioannou, P. A. (2017b). Coordinated variable speed limit, ramp metering and lane change control of highway traffic. *IFAC-PapersOnLine*, *50*(1), 5307–5312.

Zhang, Y., & Ioannou, P. A. (2017c). Integrated control of highway traffic flow. *Journal of Control and Decision*, 1–23.